

Evolution of Co charge disproportionation with Na order in Na_xCoO_2

I.R. Mukhamedshin,^{1,2,*} A.V. Dooglav,^{1,2} S.A. Krivenko,¹ and H. Alloul^{2,†}

¹*Institute of Physics, Kazan Federal University, 420008 Kazan, Russia*

²*Laboratoire de Physique des Solides, CNRS UMR 8502, Université Paris-Sud, 91405 Orsay, France, EU*

⁵⁹Co NMR experiments have been performed on single crystals of the layered cobaltate Na_xCoO_2 with $x=0.77$ which is an antiferromagnet with Néel temperature $T_N = 22$ K. In this metallic phase six Co sites are resolved in the NMR spectra, with distinct quadrupole frequencies ν_Q , magnetic shifts K_{ZZ} and nuclear spin lattice relaxation rates $1/T_1$. Contrary to the $x = 1/2$ or $x = 2/3$ phases the 3D stacking of the Na planes is not perfect for $x = 0.77$ but this does not influence markedly the electronic properties. We evidence that the magnetic and charge properties of the Co sites are highly correlated with each other as K_{ZZ} and $(1/T_1)^{1/2}$ scale linearly with ν_Q . The data analysis allows us to separate the contribution ν_Q^{latt} of the ionic charges to ν_Q from that ν_Q^{el} due to the hole orbitals on the Co sites. We could extend coherently this analysis to all the known phases in the Na cobaltate phase diagram. The variation with x of ν_Q^{latt} is found to fit rather well numerical computations done in a point charge model. The second term ν_Q^{el} allowed us to deduce the hole concentration on the cobalts. These detailed experimental results should stimulate theoretical calculations of the electronic structure involving both the Co orbital configurations and DMFT approaches to take into account the electronic correlations.

PACS numbers: 71.27.+a, 76.60.-k, 61.66.-f

I. INTRODUCTION

Among the various families of correlated electron systems the layered cobaltates Na_xCoO_2 are quite original due to the triangular arrangement of the Co atoms in the CoO_2 layers. In the CoO_6 octahedra which build up the layered structure, the strong crystal field induced on the Co lowers the t_{2g} ionic levels with respect to the e_g levels. This favors for the cobalt electronic structure the low spin configurations in which the 5 to 6 electrons on the Co reside on the t_{2g} ionic levels.¹ This electronic structure is at the origin of many singular physical properties, such as superconductivity, low T Curie-Weiss (CW) behaviour, thermoelectric properties *etc.*²

As in many layered correlated electron systems, the variation of the interlayer charge density, that is here the Na content, modifies the doping of the CoO_2 layers, which permits to span a rich phase diagram. Interestingly, initial investigations concluded that the stable Na contents correspond to phases for which the Na atoms or equivalently the Na vacancies are ordered.^{3,4} This ordering of the dopants is at variance with the case of cuprates for which the chemical dopants are quite often disordered, and for which specific new phases are apparently favoured by dopant order.

NMR/NQR experiments have proved so far to be excellent probes allowing to evidence not only the Na atomic order but also that Co charge disproportionation occurs. Indeed the ⁵⁹Co NMR data easily give evidence for the occurrence of nonmagnetic Co^{3+} sites which correspond to filled t_{2g} levels. Such sites are absent for $x < 0.5$ for which SC occurs upon insertion of water. Their concentration progressively increases with Na content for $x > 0.5$ up to full Co^{3+} content at $x = 1$. But for $0.5 < x < 1$, the concentration of Co^{3+} depends of the actual Na atomic order.²

Two specific ordered phases $x = 0.5$ and $x = 2/3$ could be studied in great detail as their structure and NMR spectra could be resolved. For $x = 0.5$ the Na atoms are ordered in an orthorhombic superstructure commensurate with the Co lattice.⁵ As a consequence a small charge disproportionation into $\text{Co}^{3.5\pm\epsilon}$ (with $\epsilon < 0.2$) occurs on the two Co sites.⁶ For the $x = 2/3$ phase NMR/NQR experiments have allowed the determination of both the 2D Na ordered structure and the 3D stacking of Na/Co planes.⁷ The Co^{3+} ions are stabilized on 25% of the cobalt sites Co1 arranged in a triangular sublattice. The holes are delocalized on the 75% complementary cobalt sites Co2 which display a planar cobalt kagomé structure, with an average charge state close to $\text{Co}^{3.5+}$. The parameters of the Zeeman and quadrupolar Hamiltonians determined for these Co2 sites have given evidence that their electronic properties drive those of this $x = 2/3$ phase.⁸

But so far it is not clear whether the original electronic properties are driven solely by the quantum state in the 2D layer or by the Na order which could help to pin this state. This question is raised as for $x \geq 2/3$ four phases have the same CW magnetic behaviour above 100 K, but very different ground states.⁹ For $x > 0.75$ the detected 3D ordered magnetic behaviour is suggestive of a role of the Na order.^{10,11}

Indeed all known phases with $x > 0.62$ have ferromagnetic in plane properties and display for $x > 0.75$ a plane to plane antiferromagnetic (AF) order at low T .^{12,13} To understand this difference in the properties one needs to determine the details of the Na order and Co charge disproportionation. This appears as a difficult task, as the control of the synthesis of samples for large x has been difficult so far as contact with humid air leads to destruction of the phase purity and loss of sodium content.¹⁴ Progresses on that respect have been

done recently by selecting one of the most reproducible phase with $T_N = 22$ K for which we could synthesise single phase crystals. From the ^{23}Na NMR study we could characterize the Na in plane order and could as well evidence by ^{59}Co NMR the existence of at least six Co sites, three of them with quite distinct magnetic properties.¹⁵

This large number of sites opens a quite interesting situation permitting to search for the correlation of the Co charge order with the magnetic properties. For that we need to get accurate determinations of the quadrupole data on each of the Co sites in order to try to distinguish the contributions to the EFG of the static and mobile charges. The detailed investigation and analysis of the ^{59}Co NMR spectra is therefore the main aim of the present paper, task which has been eased by the extensive technical expertise we have developed in our previous study of the $x = 2/3$ phase.⁸

After a brief recall in Sec. II of the experimental techniques, in Sec. III we perform detailed analysis of the ^{59}Co NMR spectra taken on single crystal samples in high magnetic field, which permits us to identify the quadrupole frequencies ν_Q for the six cobalt sites (we compare the ^{59}Co NMR spectra taken on powder and single crystal samples in Appendix A). The magnetic shift, T_1 and T_2 data are used to reveal the magnetic properties detected by the given Co atomic sites.

In Sec. IV we establish linear correlations between the quadrupolar and magnetic properties, which is an evidence for the variation of charge disproportionation on the Co sites, as discussed in Sec. V. There, the analysis of the data permits us to separate the ionic contribution to the EFG with respect to the cobalt on site delocalized charge contribution and therefore to evaluate the charge disproportionation on the diverse sites of the structure.

The extension of this analysis to the entire phase diagram of Na cobaltates permits us then to get a coherent picture of the evolution with Na content of the various parameters considered above. This allows us then to discuss the electronic structure questions which remain to be solved from the theory standpoint to describe faithfully the experimental results established so far.

II. SAMPLES AND EXPERIMENTAL TECHNIQUES

Experiments on sodium cobaltates Na_xCoO_2 with 22 K Néel temperature have been performed on both oriented powders and single crystal samples. The detailed description of the preparation methods and main characteristics of the powder sample and single crystal SC1 have been given in Ref. 16. Also a series of sodium cobaltates Na_xCoO_2 with $x \approx 0.8$ were grown independently by the floating zone technique in Kazan Federal University. Using an electrochemical Na de-intercalation method we reduced the sodium content in the as-grown crystals down to that of the pure phase with 22 K Néel temperature and $x \approx 0.77$.¹⁵ One of them was used in this study -

below we quote it as single crystal SC4.

The ^{59}Co NMR measurements were done using home-built coherent pulsed NMR spectrometers. NMR spectra were taken with $\pi/2 - \tau - \pi/2$ or $\pi/2 - \tau - \pi$ radio frequency (rf) pulse sequences. Spectra obtained by both sequences were quite similar, the only difference being the relative intensities of the quadrupolar satellites and the central line. The usual $\pi/2$ pulse length was about 2-2.5 μs depending on the coil size and the minimum practical τ value used in our experiments was 5 μs . The ^{59}Co NMR spectra were taken either in fixed field or in sweep field mode. In fixed magnetic field B_0 the NMR spectra were recorded point by point by varying the spectrometer frequency in equal frequency steps. In sweep field mode, the NMR spectrometer frequency ν_0 was fixed and the spectra were taken in an external magnetic field which was varied in equal steps. In both modes the full NMR spectra were then constructed using a Fourier mapping algorithm.^{17,18}

III. ^{59}Co NMR SPECTRA

Generally in solid state NMR an atomic nucleus with spin \vec{I} , quadrupole moment Q and gyromagnetic ratio γ has its spin energy levels determined by the Zeeman interaction with the applied magnetic field $\vec{H} = B_0/\mu_B$ and the quadrupolar interaction with the electric field gradient (EFG) on the nucleus site. The total Hamiltonian can be written as:^{19,20}

$$\mathcal{H} = \mathcal{H}_Z + \mathcal{H}_Q = -\gamma\hbar\vec{I}(1 + \hat{K})\vec{H} + \frac{eQ}{2I(I-1)}\vec{I}\hat{V}\vec{I}. \quad (1)$$

In this Hamiltonian, the magnetic shift tensor \hat{K} and the EFG tensor \hat{V} reflect the physical properties of the studied compound and are linked with the local structure. In the case where their principal axes (X, Y, Z) coincide, the Zeeman and quadrupolar Hamiltonians can be re-written:

$$\begin{aligned} \mathcal{H}_Z &= -\gamma\hbar \sum_{\alpha} I_{\alpha}(1 + K_{\alpha\alpha})H_{\alpha}; \\ \mathcal{H}_Q &= \frac{eQ}{2I(2I-1)} \sum_{\alpha} V_{\alpha\alpha}I_{\alpha}^2 \\ &= \frac{h\nu_Q}{6} [3I_Z^2 - I(I-1) + \eta(I_X^2 - I_Y^2)], \end{aligned} \quad (2)$$

where $\alpha = X, Y, Z$. Traditionally the principal axes of the EFG tensor are selected as $|V_{ZZ}| \geq |V_{YY}| \geq |V_{XX}|$. In that case the quadrupolar frequency

$$\nu_Q = \frac{3eQV_{ZZ}}{2I(2I-1)h} \quad (3)$$

corresponds to the largest principal axis component V_{ZZ} of the EFG tensor and $\eta = (V_{XX} - V_{YY})/V_{ZZ}$ reflects the asymmetry of the EFG tensor.

For a single Co site in the cell the simplest ^{59}Co NMR spectrum is detected when the principal axis of

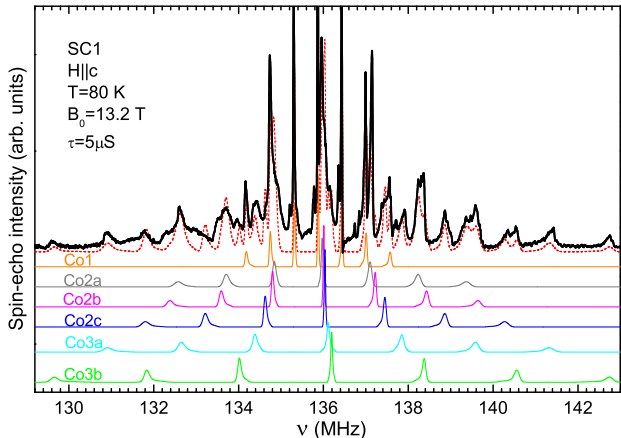


FIG. 1. (Color online) Experimental ^{59}Co NMR spectrum (top thick black line) of the SC1 sample measured in the fixed magnetic field $B_0 \parallel c$. The simulations of the spectra for 6 distinct Co sites NMR signals are shown by colour lines. The parameters used in the simulations are presented in Table I. The sum of the simulated cobalt spectra with the weight coefficients from Table I is shown by a red dotted line.

the EFG tensor Z coincides with the direction of the external applied field H . In first order perturbation theory, it consists then of seven equally spaced lines: a central line which corresponds to the $-\frac{1}{2} \leftrightarrow \frac{1}{2}$ transition and 6 quadrupolar satellites corresponding to the other $m \leftrightarrow (m-1)$ transitions which are symmetrically arranged around the central line. The frequency splitting between lines in the spectrum is equal to the quadrupolar frequency ν_Q . The position of the central line in the spectrum is determined by the K_{ZZ} component of the magnetic shift tensor.

In Fig. 1 an example of ^{59}Co NMR spectrum with good resolution taken in high applied field $B_0 \parallel c$ is shown for the SC1 sample. One can see that there is a full set of distinct satellites which can be sorted out knowing that each set of six lines are separated in frequency by a specific ν_Q for each Co site

A. Co1 sites NMR spectra

As we have shown in our early studies,²¹ the ^{59}Co NMR spectra in cobaltates strongly depend on the time interval τ between rf pulses, as the signals for the distinct sites which contribute to the NMR spectrum have different nuclear relaxation parameters. We have used that at length to separate the spectra for the sites with long and short transverse relaxation times T_2 . The existence of such a T_2 differentiation in the $T_N = 22$ K phase has already been demonstrated in Ref. 15 and can be seen in Appendix A (Fig. 5 and Fig. 6).

In the long τ spectrum the only detected signal contribution is that for the sites with the longest T_2 . We

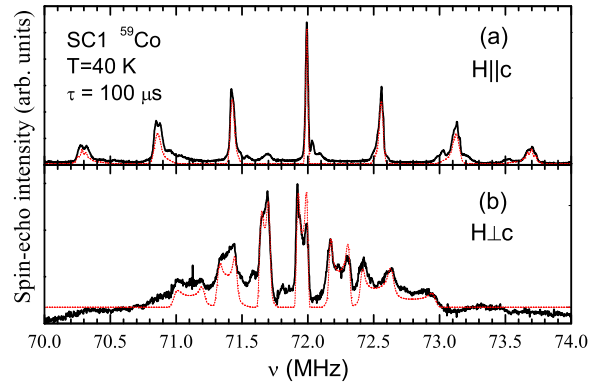


FIG. 2. (Color online) ^{59}Co NMR spectra of SC1 sample measured at long time interval $\tau = 100\mu\text{s}$ between rf pulses in the two directions of the applied magnetic field. The simulation of the spectra of Co1 are shown by the red dotted lines. See text for details.

traditionally called the corresponding cobalt sites as Co1 in most phases studied so far by NMR, and associated them with Co sites which are nearly Co^{3+} , for which the six t_{2g} sublevels are fully filled.

In Fig. 2 we show examples of long- τ spectra of the SC1 sample for $H \parallel c$ and $H \perp c$. The $H \parallel c$ spectrum displays clearly the expected seven lines spectrum which permits an easy determination of $K_{ZZ} = 2.36\%$ and $\nu_Q = 0.57$ MHz from the computer fit shown in Fig. 2(a). For $H \perp c$, the single crystal and aligned powder sample spectra are similar and some of them are shown in Fig. 6 of the Appendix A. Therefore all XY orientations are seen in the single crystal samples, which explains the complex lineshape of Fig. 2(b). The latter reflects the existence of an anisotropy of the EFG characterized by the asymmetry parameter η . Computer simulation assuming a XY random disorder permits us to determine $\eta \simeq 0.15$ from the best fit shown by a red dotted line in Fig. 2(b) (there a small broad background signal contribution can be attributed to the residual signals of the short T_2 Co sites in the structure). These simulations permitted us to evidence a small in-plane asymmetry of the magnetic shift tensor components for Co1 sites: $K_{XX} = 2.25\%$ and $K_{YY} = 2.36\%$. We further found that the in-plane XY principal axes of the magnetic shift and quadrupolar tensors are distinct and rotated by about 25° with respect to each other.

B. Simulation of the spectra for the other Co lines

We cannot do the same as for Co1 (Fig. 2) for the other Co sites, as their spectra overlap and their T_2 are similar. This is certainly impossible for $H \perp c$ (see Appendix A), but even for $H \parallel c$ we have to resort on a computer simulation to fit the spectrum using the methods we have reported previously for $x = 2/3$.⁸ We could match the six

TABLE I. Parameters used for computer simulations of the 6 contributions to the ^{59}Co NMR spectra shown in Fig. 1. K_{ZZ} and ν_Q are the magnetic shift and the quadrupolar frequency while $\Delta\nu$ and $\Delta\nu_Q$ are the widths of their respective Lorentzian distributions. I_n is the number of cobalts corresponding to the given Co site in the simulated spectrum (total number of cobalts is 13). The values of the longitudinal relaxation time T_1 and transverse nuclear magnetization relaxation time T_2 for each cobalt site, measured at $T=80$ K are listed as well.

	Co1	Co2a	Co2b	Co2c	Co3a	Co3b
K_{ZZ} , %	2.38	2.45	2.48	2.50	2.56	2.62
$\Delta\nu$, kHz	16	44	20	21	81	41
ν_Q , MHz	0.568	1.14	1.217	1.42	1.745	2.19
$\Delta\nu_Q$, kHz	15	52	41	50	50	45
I_n	3	4	1	2	2	1
T_1 , ms	2.98(3)	0.91(5)	0.75(4)	0.71(4)	0.30(1)	0.17(1)
T_2 , μs	147(4)	45(2)	47(2)	44(3)	19(1)	16(1)

quadrupole satellites associated with each component of the central line for which K_{ZZ} has been obtained.¹⁵ In all studied samples at least six sets of Co quadrupolar satellite lines could be distinguished by their ν_Q values. For each Co site the largest splitting between satellites is observed when $H \parallel c$, which evidences that the principal axis Z of the EFG tensor is close to the crystallographic c axis for all cobalts. Using the value of ν_Q for each site we could compute its contribution to the spectrum using the parameters listed in Table I.

To simulate the broadening of the experimental quadrupole satellite lines we combined the Lorentzian width $\Delta\nu$ used to fit the central line spectrum in Ref. 15 with an additional Lorentzian distribution of ν_Q with a full width at half maximum (FWHM) $\Delta\nu_Q$ - see Table I. The latter naturally reproduces the increased linewidth of the external transitions with respect to the internal ones. Finally the relative intensities of the six components have been matched using those found for the central lines, which were confirmed by accurate comparisons reported in Appendix B. Those allowed us to assign the number I_n of sites associated with each Co signal as given in Table I.

The corresponding fit summing the six contributions to the ^{59}Co NMR spectra is displayed as a dotted line in Fig. 1. Notice that the discrepancies which occur are not fortuitous as we found them highly reproducible in the spectra for different samples, as discussed in Appendix C.

IV. CORRELATION BETWEEN CHARGE AND MAGNETIC PROPERTIES

The unfilled local charge, if it is localized as in a Mott insulator, is directly linked with the ionic magnetism, while in a metal the unfilled shell participates in the conductivity and magnetic properties of the metallic state. Obviously, in our metallic systems the large variation of

ν_Q for the various Co sites is related to the local Co orbitals that participate in the metallic bands, as we have already seen for other x values.⁸ We have now in Table I the K_{ZZ} and ν_Q values which are respectively associated with magnetic and charge properties for the six sites of the Co plane, so we can test how they correlate to each other.

A. Correlation between K_{ZZ} and ν_Q

Fig. 3(a), where K_{ZZ} versus ν_Q values listed in Table I are plotted, evidence a simple linear correlation between these two quantities. On the same figure we reported the data for these quantities obtained for the four Co sites detected for $x = 2/3$.⁸ Though they do not scale as nicely with each other as for the $x = 0.77$ case, the trend is quite similar and the Co1a and Co1b sites correspond there to smaller K_{ZZ} and ν_Q than for Co2a and Co2b sites.

Conversely we have evidenced for the $x = 2/3$ phase that $K_{XX}, K_{YY} > K_{ZZ}$ on the Co2 magnetic sites.⁸ It would be important to determine if this happens as well for the magnetic sites of the $x = 0.77$ phase. For $x = 2/3$ this was seen from direct shift measurements in the $H \perp c$ direction. There we developed a full analysis which permitted us to distinguish the K_{XX}, K_{YY} contributions for the two fast relaxing sites of the structure Co2a and Co2b. As in the $x = 2/3$ phase, we can see a strong anisotropy of the shift in the $H \perp c$ spectra (see Appendix A), but those are too complicated to attempt such a differentiation for the five fast relaxing Co sites for $x = 0.77$.

B. Correlation between T_1 , T_2 and ν_Q

We have demonstrated for $x = 2/3$ that T_1 and T_2 data also allow us to detect the anisotropy of magnetic properties of the Co2 sites.⁸ We shall therefore use these quantities to further test the correlation between the magnetic properties and ν_Q for the $x = 0.77$ phase.

Due to the close values of the magnetic shift for all cobalts sites in the $H \parallel c$ direction (see Table I), to avoid cross-relaxation between sites we measured T_1 on selected quadrupolar satellite transitions of different sites which are quite separated in frequency - see Fig. 1 as example. The details of the measurements are given in Appendix D and the T_1 values measured for the different sites are listed in Table I. We do see there that $1/T_1$ increases markedly with ν_Q .

Let us recall that, in systems with unpaired spins, the dominant T_1 process is due to local field fluctuations induced by the dynamics of the local electronic magnetization.⁸ For $H \parallel c$, this T_1^{-1} is governed by the fluctuations of the transverse components of the effective magnetic field induced at the nucleus. Thus it is driven then by the K_{XX} and K_{YY} components of the magnetic shift tensor so that $T_{1Z}^{-1} \propto (K_{YY}^2 + K_{XX}^2)$. So, to probe

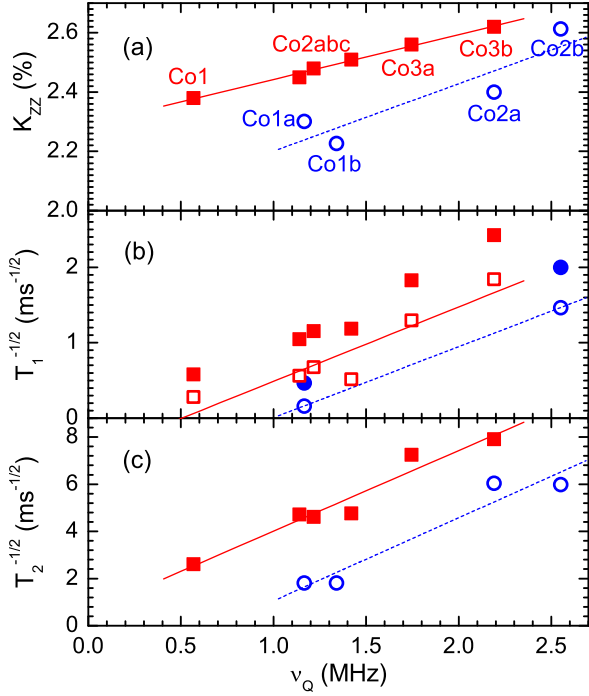


FIG. 3. (Color online) (a) K_{ZZ} , (b) $(1/T_1)^{1/2}$ (closed symbols) and $(1/T_{1spin})^{1/2}$ (open symbols) (c) $(1/T_2)^{1/2}$ vs. ν_Q for cobalt sites in $x = 0.77$ phase (red squares) and $x = 2/3$ phase (blue circles). Linear fits are shown as eyeguides.

the correlation of the transverse spin shifts with the on site charge, it appears practical to plot $(1/T_{1Z})^{1/2}$ versus ν_Q , as done in Fig. 3(b). There one can see that a clear linear relation holds amazingly for the six sites and can by no way be considered as fortuitous. This plot means that the transverse spin shifts K_{XX} and K_{YY} do scale as well with ν_Q or K_{ZZ} . Therefore the large T_1^{-1} values found for the Co3 sites with large ν_Q values clearly confirm the magnetic character of these cobalt sites.

The transverse relaxation rate $(1/T_2)^{1/2}$ displays a similar scaling as shown in the plot of Fig. 3(c), which means that it is dominated by the T_1 process.

Although the scaling is clear, the ratio of $(1/T_1)^{1/2}$ for Co3a and Co3b is only about 1.3 and the three Co2 sites have similar T_1 values. Therefore the rough distinction done from the T_2 data in Ref. 15 between the three types of sites Co1, Co2 and Co3 is maintained. Co1 is close to nonmagnetic Co^{3+} , Co3a and Co3b sites are the most magnetic cobalt sites in this $x=0.77$ phase, and the remaining three Co2 sites display an intermediate behaviour.

V. DISCUSSION

To explain a linear variation of the Knight shift K_{ZZ} with ν_Q (Fig. 3(a)) let us consider the significance of these measured physical quantities.

The quadrupole frequency ν_Q is proportional to the largest component of the EFG tensor \hat{V} (Eq. (3)). The components of ν_Q and \hat{V} can be written as the sums of two contributions

$$\nu_Q = \nu_Q^{latt} + \nu_Q^{el} \quad (4)$$

$$\hat{V} = (1 - \gamma_\infty) \hat{V}^{latt} + (1 - R_{el}) \hat{V}^{el}. \quad (5)$$

The first term in Eq. (5), which gives the lattice contribution to ν_Q arises from all ion charges outside the ion under consideration, enhanced by the core electrons of the atom by Sternheimer antishielding factor γ_∞ . The second term in Eq. (5) gives the local electronic contribution to ν_Q and arises from unfilled electron shells of the orbitals of the considered site. Those induce distortions of the inner electronic orbitals embedded in the value of $(1 - R_{el})$ which usually just slightly smaller than unity.

For an isolated ionic site in an insulator the EFG tensor for one hole on t_{2g} orbitals would be expressed as^{22,23}

$$\hat{V}^{el} = -\frac{2}{21} \langle r^{-3} \rangle e\hat{q}, \quad (6)$$

where $\langle r^{-3} \rangle$ is the expectation value of r^{-3} for the $3d$ electron and $e\hat{q}$ is the electric quadrupole moment of the t_{2g} hole. The on-site spatial distribution of the hole is represented by the second-rank tensor \hat{q} , given by the expectation value of the operators $q_{\alpha\beta} \equiv \frac{3}{2}(L_\alpha L_\beta + L_\beta L_\alpha) - \delta_{\alpha\beta} L^2$ ($\alpha, \beta = x, y, z$) where L is the orbital momentum.²³

In the metallic state constructed from the low spin ionic configuration of the Co one has to take into account solely the contribution of the Co orbitals involved in the metallic band up to the Fermi level, so that the on site charge δ , corresponding to the disproportionated charge in chemistry language, has to be introduced as a multiplicative factor in Eq. (6). For simplicity δ might be embedded in the definition of \hat{q} , which would represent then the local charge concentration weighted by an anisotropy of the angular distribution of electronic density. This local charge term is important as it represents a direct on site signature of the electronic structure. For instance for the Co^{3+} low spin state with a fully filled t_{2g} multiplet the local electronic structure is isotropic and should not contribute to \hat{V}^{el} and ν_Q^{el} .

The magnetic shift tensor \hat{K} reflects the additional magnetic fields on the nuclear site which could be written in terms of the spin \vec{S} and orbital \vec{L} operators:^{22,23}

$$\hat{K}\vec{H}_0 = -2\mu_B \langle r^{-3} \rangle (\vec{L} - \kappa \vec{S} + \frac{2}{21} \hat{q} \vec{S}). \quad (7)$$

Here μ_B is the Bohr magneton and the orbital contribution to the shift has been separated from the spin contribution.

The first term in Eq. (7) describes the magnetic interaction between the nuclear spin and the d -orbital moment. The second contribution corresponds to the isotropic contact Fermi coupling of the nucleus spin to

the spin polarization of the inner s -electrons shells induced by the outer d electrons (core polarization). The third term in Eq. (7) describes the magnetic dipolar interaction between the nuclear spin and the quadrupolar part $\hat{q}\vec{S}$ of the distribution of the t_{2g} -hole spin density.²²

It is important that both measured values ν_Q and \hat{K} contain terms proportional to the quadrupole moment of the t_{2g} hole density distribution \hat{q} which involves as a coefficient the hole concentration δ on the Co site. Therefore the linear variation with ν_Q found for the Knight shift K_{ZZ} and $(T_1)^{-1/2}$ just reflects the fact that the hole content on the Co orbitals varies from site to site in this $x = 0.77$ phase. Also this observation means that the hyperfine coupling, or the local magnetic χ scales with the on site delocalized charge.

A. Estimation of the charge disproportionation for the different Co sites

The second term in Eq. (5) is clearly linked with the Co on site hole occupancy, and does vanish in the Co^{3+} low spin state with six electrons filling the t_{2g} orbitals. Such Co atoms being nonmagnetic, we do expect their T_1 to become extremely long as observed experimentally.^{21,24,25}

Therefore in the plot of Fig. 3(b) the pure Co^{3+} state should correspond to $(1/T_1)^{1/2} \rightarrow 0$ so that the corresponding $\nu_Q = \nu_0 \simeq 0.2 \text{ MHz}$ should be solely due to the lattice contribution ν_Q^{latt} to the EFG. We can therefore anticipate that the quantity $\nu_Q - \nu_0$ is directly related on each site with the local charge term in Eq. (5).

It therefore measures the charge disproportionation on the different sites of the structure, and we could write $\delta_n = A(\nu_{Q,n} - \nu_0)$ for a site n with quadrupolar frequency $\nu_{Q,n}$ and charge $3 + \delta_n$. Knowing the number I_n of sites n in the unit cell the charge neutrality implies

$$A \sum I_n (\nu_{Q,n} - \nu_0) = (1 - x) \sum I_n. \quad (8)$$

The data for $\nu_{Q,n}$ and I_n obtained from the signal intensity analysis given in Table I therefore permit us to determine δ_n values listed in Table II. These estimates would indicate that the disproportionation ranges from $\text{Co}^{3.08+}$ for the Co1 sites, with an average of $\text{Co}^{3.24+}$ on the Co2 sites and an average of $\text{Co}^{3.40+}$ for the Co3 sites.

We did for $x = 2/3$ an equivalent analysis based on the values of ν_Q for the Co sites of the kagomé structure.⁸ It is reproduced in Fig. 3(b), which gives $\nu_0 \sim 0.7 \text{ MHz}$ and the δ_n values listed in Table II.

In fact, for completeness we have to take into account that the measured T_1 involves an orbital contribution $1/T_{1orb}$ which we evidenced explicitly for $x = 2/3$ in Ref. 8. As the δ_n values (Table II) varies in the same range for both $x = 0.77$ and $x = 2/3$ phases and $1/T_1$ values for cobalts are also quite close, we assumed that for the $x = 0.77$ phase the $1/T_{1orb}$ versus ν_Q dependence has the same slope as for the $x = 2/3$ phase which allowed us

TABLE II. Hole concentration δ deduced from the analysis of the correlation between $(1/T_1)^{1/2}$ and ν_Q data for different cobalt sites with charge states $\text{Co}^{3+\delta}$ in $x = 2/3$ and $x = 0.77$ phases. In the tables, the upper values of ν_0 are obtained from the raw data and the lower ones after subtracting the orbital contribution to $1/T_1$, as displayed in Fig. 3(b)

$x=2/3$						
ν_0 , MHz	Co1a	Co1b	Co2a	Co2b		
0.7	0.11	0.15	0.35	0.43		
1.0	0.05	0.10	0.35	0.46		
$x=0.77$						
ν_0 , MHz	Co1	Co2a	Co2b	Co2c	Co3a	Co3b
0.2	0.08	0.21	0.23	0.27	0.35	0.45
0.5	0.02	0.20	0.23	0.29	0.39	0.53

to estimate $1/T_{1orb}$ for all Co sites in the $x = 0.77$ phase. In Fig. 3(b) we report the spin contributions $1/T_{1spin}$ to the relaxation for both phases after subtracting the orbital term. We find that using $(1/T_{1spin})^{1/2} \rightarrow 0$ only induces a $\approx 0.3 \text{ MHz}$ increase of ν_0 values for both 0.77 and 2/3 phases. As can be seen in Table II this does not change significantly the δ_n values except for the Co1 sites which become closer to Co^{3+} .

The slope of $(1/T_{1spin})^{1/2}/\nu_Q$ is found quite similar in Fig. 3(b) for both samples. This can be ascribed to the analogous T variations of $1/T_1$ found for such phases above 80 K.⁹ Finally a similar analysis of low T NQR data taken on the O71 sample, which is detailed in Appendix E also gives a distinction between two types of sites and very similar values as for the two sites for $x = 2/3$. So the comparison of these three cases leads us to the conclusion that for $x < 0.75$ the disproportionation to nearly nonmagnetic Co^{3+} and magnetic $\text{Co}^{\approx 3.5+}$ sites happens. The disproportionation appears more complex for the $x = 0.77$ phase as apart Co^{3+} two differently charged states are involved.

B. Evolution of the ionic contribution to ν_Q in the phase diagram

One can expect that the ν_Q^{latt} contribution to ν_Q changes with Na content and order. In rectangular coordinates the components of corresponding \hat{V}^{latt} tensor can generally be calculated in a point charge model

$$V_{\alpha\beta}^{latt} = \sum_i q_i \left(\frac{3\alpha_i\beta_i - r_i^2\delta_{\alpha\beta}}{r_i^5} \right), \quad (9)$$

where q_i is the charge of the ion i , located with respect to the probe nucleus at the vector \vec{r}_i with components α_i and β_i with $\alpha, \beta = X, Y, Z$.

So ν_Q^{latt} can be estimated in a first step without taking into account the Na order and the Co charge disproportionation. We performed a simple point charge calculation, assuming a homogeneous distribution of ionic charge on the Na sites (that is a charge x on every Na2 site), charges -2 on all O sites and $4-x$ on each Co.²⁶ This

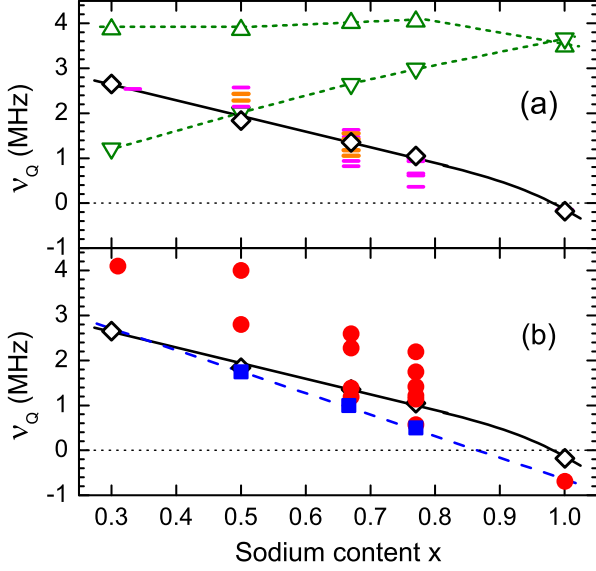


FIG. 4. (Color on line) (a) The lattice contribution to the quadrupole frequency variation ν_{Q0}^{latt} (black open diamonds and black line) computed for a uniform distribution of Na and Co sites. It results from the contributions ν_{QA} and ν_{QB} (green open up and down triangles correspondingly). Using the actual Na order yields the differentiation of ν_Q^{latt} values on the Co sites given by horizontal magenta ticks. Including the Co charge disproportionation slightly reduces this differentiation (orange ticks) and only slightly modifies the average magnitude of the computed ν_Q^{latt} values with respect to the uniform case. (b) Comparison of the experimental ν_Q data (red full circles) with point charge calculations. The $\nu_0(x)$ values deduced from the analyses of Fig. 3(b) (blue closed squares and dashed line) parallels the variation of the computed data. See text for details.

resumes into calculating the contributions ν_{QA} (Na2:0; O:-2; Co:4) which represents the contribution of the non-charged CoO_2 layers and ν_{QB} (Na2: x ; O:0; Co:- x) representing the Na and hole contributions to the EFG.

The calculated $\nu_{Q0}^{latt} = \nu_{QA} + \nu_{QB}$ on the cobalt sites is plotted versus x in Fig. 4 using the cell parameters known from refinements of x-ray data.^{5,24,27–29}

To further test the validity of our analyses of the data we need to appreciate the soundness of the evolution with Na content of ν_0 which we have also plotted in Fig. 4.

There one can see that the variation with x of ν_{Q0}^{latt} has a similar regular decrease with x as that displayed by $\nu_0(x)$, though the computed values are slightly larger. Of course the existence of Na order and charge disproportionation might justify this difference. As the Na order unit cell is perfectly known for $x = 1/2$ and $x = 2/3$, we therefore could compute ν_Q^{latt} for those phases. The computed values on the distinct Co sites do not correspond to a single value and deviate from ν_{Q0}^{latt} . However the differentiation between the computed ν_Q^{latt} values is reduced if one takes also into account the Co charge dis-

proportionation determined above from the analysis of the experimental ν_Q values.

We computed also the expected ν_Q^{latt} for a hypothetical triangular arrangement of Na ions on Na2 sites for $x = 1/3$. Similarly for the $x = 0.77$ phases we calculated ν_Q^{latt} for different stacking along c -axis of 2D Na order pattern established in Ref.¹⁶ Despite the uncertainty in the 3D stacking the trend in the variation of $\nu_Q^{latt}(x)$ remains similar.

In Fig. 4 we have reported as well the experimental ν_Q values for the various Co sites identified for the studied Na contents. As expected these data are mostly above the computed values, whatever the approximation done, as the local charge contribution ν_Q^{el} of the unfilled Co orbitals does of course contribute to ν_Q .

One puzzling result is that for $x = 1$, the calculated value of ν_Q^{latt} is also found below the experimental result, while in this insulating band case one does not expect any ν_Q^{el} contribution. When trying to clarify that point we noticed that in the homogeneous charge model, ν_{QA} and ν_{QB} are of opposite sign and nearly compensate each other for $x = 1$. This explains the difficulty to fit the $x = 1$ data, as the Co-O hybridization might yield deviations from point charge calculations for the contribution ν_{QA} of the CoO_2 slabs.

We may notice that for most Na contents the computed values for ν_Q^{latt} are always slightly above the actual $\nu_0(x)$ values, so that one might consider that ν_{QA} is always slightly overestimated. We are then led to conclude that $\nu_0(x)$ values are rather good determinations of ν_Q^{latt} . This could mean that the actual value of ν_Q for $x = 1$ would be negative, as the sign of the EFG is not accessible experimentally. In such a case the variation of $\nu_0(x)$ would smoothly extend linearly up to $x = 1$ as shown in Fig. 4.

All this gives some weight to the hypothesis of Eq. (8) that a single ν_0 can be used for all Co sites to describe the disproportionation for a given Na content. This approximation is certainly not fully valid for the most stable ordered Na phases, such as $x = 2/3$ for which the differentiation between Co sites is slightly influenced by the Na order.

C. Hole contribution to ν_Q on the Co nuclei

The variation of ν_Q with the local charge δ is given by $d\nu_Q/d\delta = A^{-1}$ (A is defined in Eq. (8)). For the ν_0 values corresponding to $(1/T_1)^{1/2} \rightarrow 0$ we obtain 4.3 MHz and 4.5 MHz per on site charge for $x = 2/3$ and $x = 0.77$ respectively, while we do obtain 3.4 MHz and 3.2 MHz for the ν_0 values taken for $(1/T_{1spin})^{1/2} \rightarrow 0$. Recognizing the roughness of our model one could retain a reasonable value of 3.3 MHz per hole on Co site.

For phases with the $1/2 < x < 2/3$ the weak T variations of the NMR shifts and the lower resolution of the ^{59}Co powder spectra did not permit to get accurate data in which all sites could be identified.² But it has been shown that the concentration of non magnetic

CoI like sites decreases with decreasing x and vanishes at $x = 0.5$. In that well ordered phase the two sites differentiated correspond to $\text{Co}^{3.5+\varepsilon}$ and $\text{Co}^{3.5-\varepsilon}$.⁶ Providing we keep the same $d\nu_Q/d\delta=3.3$ MHz per hole as for higher x , the 2.8 MHz and 4 MHz measured ν_Q values allow us to estimate $\varepsilon = 0.18$. This correspond then to $\nu_0(0.5) = 1.75$ MHz which is quite close to that computed for $\nu_Q^{latt}(x = 1/2)$ - see Fig. 4. Therefore, we find that the computed ionic contribution $\nu_Q^{latt}(x)$ is reliable, and may be slightly improved by using the value $\nu_0(x)$ deduced from the analysis of the charge disproportionation.

As for the extra contribution due to the local charge ν_Q^{el} , it corresponds to about 3.3 MHz per on site charge for the variations of ν_Q on the various sites of the $x = 2/3$ and $x = 0.77$ phases, but also is compatible with the data on the $x = 1/2$ phase. The occurrence of such local charge contribution implies that the local charge is not evenly distributed on the Co t_{2g} orbitals.

Let us now evaluate the EFG which should results from a single electron or hole residing in one t_{2g} orbital, employing Eqs. (3) and (5). The magnitude of the largest component of the quadrupole moment tensor for the orbital state was calculated as $|\hat{q}| \approx 6$.²³ In the free-ion limit for Co^{4+} the coefficient $\langle r^{-3} \rangle$ has been estimated as 7.421 a.u.²² Because of a hybridization with the ligands in the sodium cobaltates this value becomes smaller, and $\langle r^{-3} \rangle = 5$ a.u. could be used as a realistic approximation. Substituting these quantities into Eqs. (3) and (5) and taking $R_{el} \ll 1$, we obtain $\nu_Q^{el} \approx 20$ MHz per single orbital for ^{59}Co . Similar values of EFG could remain in the case of a robust orbital order in the d -lattice. Such ordering could appear when the orbitals are locked by a local crystal field with a broken cubic symmetry.³⁰ In the cobaltates such field could originate from a deformation of the Co-O octahedra and/or from a low-symmetric sodium structure. For example a trigonal distortion of the oxygen octahedra induces a a_{1g} state of the Co^{4+} sites.³¹

The calculated quadrupolar frequency is about six times larger then the corresponding experimental value 3.3 MHz per Co site established in our analysis above. This suggest that in the cobaltates the holes are distributed over the three orbital states within the t_{2g} -shells due to the thermal/quantum fluctuations.³¹ Such effect could explain the recovery of the isotropy of the local wave functions.^{30,32} A plausible possibility for the reduction could come from the band structure of the holes in the triangular CoO_2 layers, which would intermix the three planar t_{2g} orbitals (xy, yz, xz).^{33,34} The quantitative description of this situation is a challenge for future theoretical developments.

VI. CONCLUSION

We have evidenced here that the ^{59}Co NMR spectrum reflects in the paramagnetic state the diverse Co sites

pertaining to the Na ordered phases in the Na cobaltates. We demonstrated that, for the $x = 0.77$ phase with $T_N = 22$ K, the Co charge disproportionation differentiates magnetically three type of sites, while for $2/3 < x < 0.75$ only two types of magnetic behaviour occur. Furthermore we could establish here that for $x = 0.77$ the charge disproportionation and the local magnetic behaviour on the Co sites are very well correlated.

The atomic structure of this $x = 0.77$ phase corresponds to a Na order which involves Na tri-vacancies and triangles of NaI sites rather than the di-vacancies and isolated NaI sites found for lower x .¹⁶ We did also find here that the stacking of the Na order is far from being perfectly locked between layers, which means that the potential which pins the Na charges does not involve very deep minima. Our analysis of the EFG on the Co sites also reveals that the lattice contribution to the EFG is quite smaller for this phase than for the phases with lower Na content.

We therefore are lead to suggest that all these phenomena are related and that the lower structural stability and the difference in the electronic properties are linked. The magnetic order being robustly found at $T_N = 22$ K by most authors, for samples of different qualities, appears insensitive to the actual stacking of the Na planes. This would mean that the overall AF interaction between Co layers is rather well defined and not dependent on the actual Na 3D order. On the contrary, this would surprisingly mean that the perfect 3D order of the Na found in the $x = 2/3$ phase would lead to a weak magnetic interaction between Co layers. This would be required to explain the absence of magnetic order and the large variation of spin susceptibility found down to $T = 50$ mK in that phase.⁹

As for the electronic properties, we evidenced that the hole contribution to the EFG and NMR shifts on the Co sites are much smaller than expected for a single t_{2g} orbital. The magnitude of the contribution per hole on the Co does not appear to change significantly with Na content. This implies that the hybridization of t_{2g} orbitals involved in the electronic structure does not change markedly with hole doping of the Co band. This would indicate that although the Na ordering probably permits to pin the charge disproportionation and to reveal it through our NMR/NQR techniques, it does not play a large role in the electronic structure, which might be an intrinsic property of the CoO_2 layers. We believe that this result simplifies the modelling of the electronic structure and that computations involving both the LDA starting point and taking into account the electronic correlations based on DMFT would be able to better describe such an experimental situation.

VII. ACKNOWLEDGMENTS

We would like to thank here F. Bert, P. Mendels and J. Bobroff for their help on the experimental NMR techniques and for constant interest and stimulating discussions. S.A.K is indebted to L.R. Tagirov for elucidating communications. I.R.M. thanks for the support of a visit to Orsay by “Investissements d’Avenir” LabEx PALM (ANR-10-LABX-0039-PALM). This study was partially supported by the Russian Foundation for Basic Research (project 14-02-01213a) and by the Program of Competitiveness Growth of Kazan Federal University funded by the Russian Government. The work of S.A.K. was supported by the Ministry of Education and Science of the Russian Federation (state order 2014/57).

Appendix A: NMR spectra for $H \parallel c$ and $H \perp c$

Figure 5 shows the NMR spectra measured in the two different single crystals and in the oriented powder sample at different temperatures with the direction of the applied magnetic field H parallel to the crystallographic c -axis of the sample ($H \parallel c$). The quadrupolar satellite lines are easily seen in such spectra which reveal a large multiplicity of Co sites with distinct EFG values. The $H \parallel c$ spectra of the single crystals samples SC1 and SC4 display identical features as that of the powder sample, with a slightly better resolution and slightly narrower satellite lines - see Fig. 5. This indicates that the c axis orientation is better defined in the single crystals, which were easily cleaved, while perfect alignment of the c axes of the single crystal grains of the powder is harder to achieve. Therefore the single crystals spectra are more useful and discussed in details in this paper.

When the external field is applied in the $H \perp c$ direction the ^{59}Co NMR spectra are very complex, even in the single crystal samples - see Fig. 6. As was shown from the ^{23}Na NMR study done in Ref. 16, the SC1 sample is not a single crystal in the $a-b$ plane and contains at least many twin boundaries and more probably a mosaic of crystallites with different orientations in plane. As a consequence in the $H \perp c$ direction the SC1 ^{23}Na and ^{59}Co NMR spectra appear quite analogous to the powder sample spectra. The SC4 $H \perp c$ spectrum has sharper features which proves more perfect in-plane order in this sample than in SC1, but mosaicity still remains in that sample.

Appendix B: Intensity analysis

To obtain the final simulated spectrum, which is shown by red line in Fig. 1, the separate contributions were summed with the weights shown in the Table I. These numbers were obtained by careful studies of specific parts of the experimental spectrum. For example, as one can see in Fig. 1 the two well resolved lines in

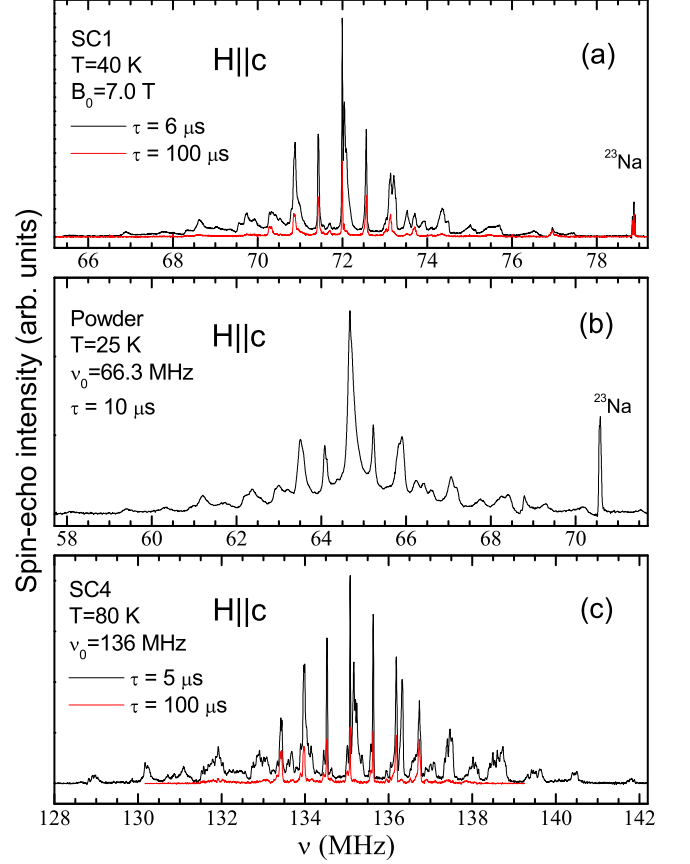


FIG. 5. (Color online) ^{59}Co NMR spectra taken with the applied magnetic field $H \parallel c$ in different samples and experimental conditions: (a) Single crystal SC1 measured at $T=40$ K in the fixed magnetic field $B_0=7$ T. Spectra measured at short time interval $\tau=6\mu\text{s}$ between rf pulses (black line) and long $\tau=100\mu\text{s}$ (red line) are shown; (b) Powder sample measured at $T=30$ K, $\tau=10\mu\text{s}$ and in sweep field mode with $\nu_0=66.3$ MHz; (c) Single crystal SC4 measured at $T=80$ K in the sweep field mode with $\nu_0=136$ MHz. Spectra measured at $\tau=5\mu\text{s}$ (black line) and $\tau=100\mu\text{s}$ (red line) are shown.

the low or high frequency parts of the spectrum corresponds to the $\pm\frac{5}{2} \leftrightarrow \pm\frac{7}{2}$ satellite transitions of the Co3a (≈ 130.9 MHz and ≈ 141.3 MHz) and Co3b (≈ 129.6 MHz and ≈ 142.8 MHz) NMR signals. To obtain their relative intensities they were integrated and the results were corrected by the transverse nuclear magnetization relaxation effects (T_2 correction). This analysis gives an intensity ratio $\text{Co3a}/\text{Co3b}=2/1$ with better than 5% accuracy. The $-\frac{3}{2} \leftrightarrow -\frac{5}{2}$ transitions of the Co2c (≈ 138.8 MHz) group are also well separated in the ^{59}Co NMR spectrum (see Fig. 1). Taking into account the relative intensities of the $\pm\frac{3}{2} \leftrightarrow \pm\frac{5}{2}$ and $\pm\frac{5}{2} \leftrightarrow \pm\frac{7}{2}$ quadrupolar satellites and the T_2 corrections we deduced that the intensities of the Co2c and Co3a are almost equal (with about 20 % accuracy). Next we determined the intensities of the $\pm\frac{5}{2} \leftrightarrow \pm\frac{7}{2}$ transitions of the Co1 (135.5 MHz

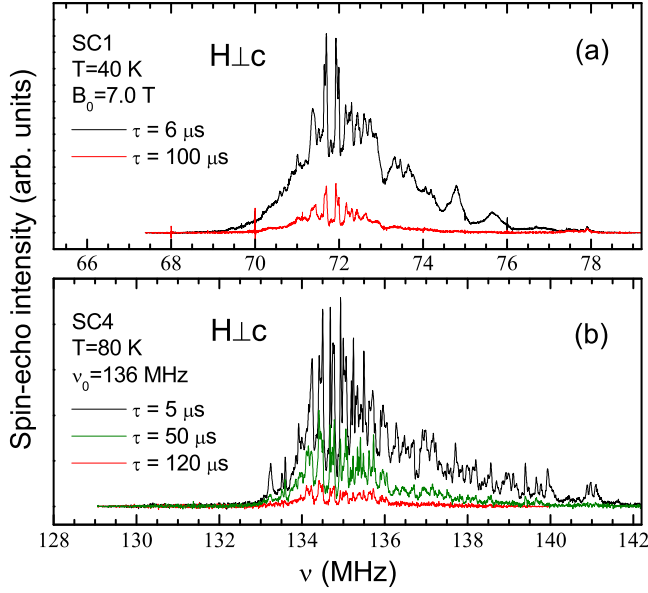


FIG. 6. (Color online) ^{59}Co NMR spectra measured in $H \perp c$ orientation: (a) Single crystal SC1 measured at $T=40$ K in the fixed magnetic field $B_0=7$ T. Spectra measured at short time interval $\tau = 6\mu\text{s}$ between rf pulses (black line) and long $\tau = 100\mu\text{s}$ (red line) are shown; (b) Single crystal SC4 measured at $T=80$ K in the sweep field mode and $\nu_0 = 136$ MHz. Spectra measured at $\tau = 5\mu\text{s}$ (black line), $\tau = 50\mu\text{s}$ (green line) and $\tau = 120\mu\text{s}$ (red line) are shown.

and 137 MHz) which are well separated in the spectrum measured at long time interval $\tau = 100\mu\text{s}$ between rf pulses (see Fig. 2), and compared their intensity with the same transitions of Co3a. After T_2 correction, this gave us the intensity ratio $\text{Co1}/\text{Co3a}=3/2$.

Finally, we established earlier on the same $x = 0.77$ samples that the two-dimensional structure of the Na order corresponds to 10 Na sites on top of a 13 Co sites unit cell.¹⁶ The intensity analysis of the central line ($-\frac{1}{2} \leftrightarrow +\frac{1}{2}$) of the ^{59}Co NMR spectrum allowed us to deduce that the ratio of the Co1 to the total cobalt NMR intensity is equal to 20(3)%.¹⁵ This number corresponds very well to 3 Co sites over 13 expected for the unit cell. Using the relative intensities which we found above we deduce that Co2a and Co2b would correspond to the five remaining Co sites. By comparing quadrupolar satellites for these lines we came to the conclusion that their intensity corresponds to $\text{Co2a}/\text{Co2b}=4/1$, this ratio remaining the most inaccurate in this intensity analysis and the ratio $\text{Co2a}/\text{Co2b}=3/2$ couldn't be completely excluded.

Appendix C: Quadrupolar satellites substructure

As one can see in Fig. 1 the agreement between the simulated spectrum and the experimental one can be considered as very good. Does that mean indeed that the structure of this $T_N = 22$ K phase does correspond

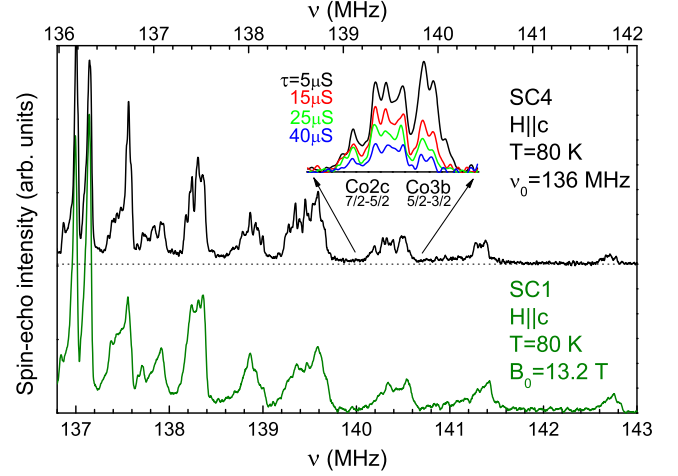


FIG. 7. (Color online) Comparison of the part of $H \parallel c$ ^{59}Co NMR spectra of the SC1 (lower panel) and SC4 (upper panel) samples measured at $T=80$ K. In the inset of upper panel we show the same group of satellite lines measured at different time interval τ between rf pulses which proves that the observed substructure is not associated with experimental noise but come from effects due to differences in the stacking of the Na layers.

to a single crystal unit cell including two CoO_2 planes and 13 Co per planar unit cell? The following detailed examination of our NMR spectra and comparisons with the data on the $x = 2/3$ phase lead us to question that possibility.

In Figure 7 we display a magnified part of the experimental ^{59}Co NMR spectra in the SC1 and SC4 samples. As one can see the quadrupolar satellites which we considered so far in Fig. 1 as single lines with some noise, do in reality represent groups of lines with slightly distinct ν_Q values. This is valid for all Co2 and Co3 NMR signals considered in those spectra. Such a sub-splitting has not been seen for Co1.

Therefore the values of the quadrupolar frequency ν_Q listed in the Table I for the various Co2 and Co3 lines should be considered as average ν_Q values for groups of Co sites with quite similar local structure and $\Delta\nu_Q$ represents the distribution of the EFG values inside each group. Also the magnetic shift K_{ZZ} values in the Table I are the values of center of symmetry position for the quadrupolar satellites for the group of Co sites. This scattering means that the 3D order is not perfect and that some defects are present but that the charge disproportionation is not so much affected by the 3D order.

Appendix D: Spin lattice relaxation of the cobalt sites

We have already shown that the magnetic sites can be differentiated by their magnetic shifts K_{zz} and by their T_2 values given in Ref. 15 from central line stud-

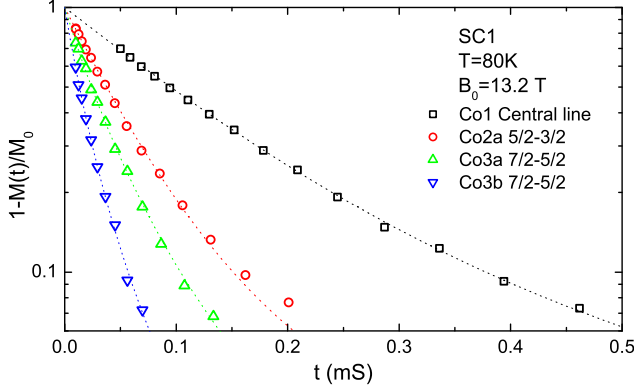


FIG. 8. (Color online) Spin-lattice relaxation curves measured on different cobalt sites in SC1 sample in the same experimental conditions as spectrum in Fig. 1. The fits of the data with the magnetization relaxation functions from Ref. 8 with parameters from the Table I are also shown.

ies. Alternatively as we have shown in Refs. 8 and 28 the magnetic sites can be differentiated by their T_1 relaxation times. Due to the close values of the magnetic shifts for all cobalts sites in the $H \parallel c$ direction (see Table I), to avoid cross-relaxation between sites we took T_1 data on quadrupolar satellite transitions of different sites which are quite separated in frequency - see for example Fig. 1. The experimental technique used for spin-lattice relaxation measurements and the relaxation functions for the different transitions for a nuclear spin $I = 7/2$ have been reported in detail previously.⁸ In Fig. 8 we show some of the longitudinal nuclear spin magnetisation decays. There the fits of the data which permit to determine the T_1 values are also reported. The deduced T_1 values are listed for all cobalt sites in Table I.

Here again the Co1 has the longest relaxation time T_1 which confirms the non-magnetic character of this cobalt site. Co3a and Co3b have rather short T_1 values as expected for magnetic Co site behaviour, and all Co2's have quite similar T_1 values in between those of Co1 and Co3b.

Appendix E: O71 Phase

We have evidenced the existence of three stable phases for $x = 2/3$, $x = 0.71$ and $x = 0.72$.^{9,14} We did not study in detail the ^{59}Co NMR spectrum for the two latter ones, but their difference has been well established by NQR

experiments.³⁵ For $x = 0.71$ the ^{59}Co NQR data allowed us to resolve at $T = 5$ K eleven Co sites with distinct ν_Q values, which are different from those of the $x = 2/3$ and $x = 0.72$ phase.¹⁴ So we could compare $1/T_1$ data measured at 4.2 K in $x = 0.71$ phase with those of the four NQR lines in the $x = 2/3$ phase taken in similar conditions - see Fig. 9.

We see that in the $x = 0.71$ phase we have fast relaxing sites with a significant scatter ($\pm 20\%$) of values of ν_Q and

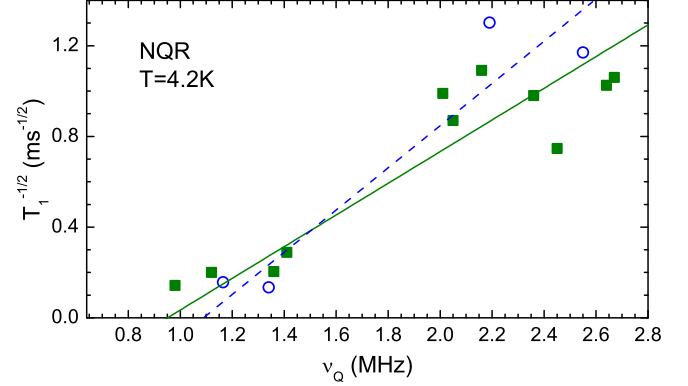


FIG. 9. (Color online) $(1/T_1)^{1/2}$ vs. ν_Q for different cobalt sites in $x = 2/3$ (open blue circles) and $x = 0.71$ (green full squares) phases measured in NQR experiments at $T=4.2$ K. Linear fits are shown by solid lines with corresponding colour.

of $(1/T_1)^{1/2}$ but the trend of this quantity versus ν_Q is identical to that found for the $x = 2/3$ phase (see Fig. 9). Furthermore the numerical values are very similar for the two phases. Here again this means that the ν_Q values distinguish 11 sites, but only two markedly distinct magnetic properties similar to Co1 and Co2 in the $x = 2/3$ phase are revealed from the $(1/T_1)^{1/2}$ versus ν_Q plots. If we just restrict the data to the weighted averages of these Co1 like and Co2 like sites one gets from the NQR data a vanishing value of $(1/T_1)^{1/2}$ for $\nu_0 \simeq 0.95$ MHz which would be associated with the non magnetic Co^{3+} . In the same experimental conditions the NQR data for $x = 2/3$ yields as well $\nu_0 \simeq 1.08$ MHz in agreement with the value obtained from the higher temperature NMR data. A correction for the orbital contribution to T_1 is not required in that case as the spin term contribution increases at low T and becomes dominant.

Here the slope of linear fits is larger by a factor 1.4 for $x = 2/3$ with respect to $x = 0.71$. This is consistent with the ratio of 1.6 found at 5 K from ^{23}Na NMR data for $(1/T_1)^{1/2}$.⁹

* Irek.Mukhamedshin@kpfu.ru

† alloul@lps.u-psud.fr

¹ D. J. Singh, Phys. Rev. B **61**, 13397 (2000).

² G. Lang, J. Bobroff, H. Alloul, G. Collin, and N. Blanchard, Phys. Rev. B **78**, 155116 (2008).

³ H. W. Zandbergen, M. L. Foo, Q. Xu, V. Kumar, and

R. J. Cava, Phys. Rev. B **70**, 024101 (2004).

⁴ Y. Hinuma, Y. S. Meng, and G. Ceder, Phys. Rev. B **77**, 224111 (2008).

⁵ A. J. Williams, J. P. Attfield, M. L. Foo, L. Viciu, and R. J. Cava, Phys. Rev. B **73**, 134401 (2006).

⁶ J. Bobroff, G. Lang, H. Alloul, N. Blanchard, and

- G. Collin, Phys. Rev. Lett. **96**, 107201 (2006).
- ⁷ H. Alloul, I. R. Mukhamedshin, T. A. Platova, and A. V. Dooglav, EPL (Europhysics Letters) **85**, 47006 (2009).
- ⁸ I. R. Mukhamedshin and H. Alloul, Phys. Rev. B **84**, 155112 (2011).
- ⁹ H. Alloul, I. R. Mukhamedshin, G. Collin, and N. Blanchard, EPL (Europhysics Letters) **82**, 17002 (2008).
- ¹⁰ J. Sugiyama, J. H. Brewer, E. J. Ansaldo, H. Itahara, T. Tani, M. Mikami, Y. Mori, T. Sasaki, S. Hébert, and A. Maignan, Phys. Rev. Lett. **92**, 017602 (2004).
- ¹¹ P. Mendels, D. Bono, J. Bobroff, G. Collin, D. Colson, N. Blanchard, H. Alloul, I. Mukhamedshin, F. Bert, A. Amato, and A. D. Hillier, Phys. Rev. Lett. **94**, 136403 (2005).
- ¹² S. P. Bayrakci, I. Mirebeau, P. Bourges, Y. Sidis, M. Enderle, J. Mesot, D. P. Chen, C. T. Lin, and B. Keimer, Phys. Rev. Lett. **94**, 157205 (2005).
- ¹³ L. M. Helme, A. T. Boothroyd, R. Coldea, D. Prabhakaran, D. A. Tennant, A. Hiess, and J. Kulda, Phys. Rev. Lett. **94**, 157206 (2005).
- ¹⁴ T. A. Platova, I. R. Mukhamedshin, A. V. Dooglav, and H. Alloul, JETP Lett. **91**, 421 (2010).
- ¹⁵ I. R. Mukhamedshin, I. F. Gilmudinov, M. A. Salosin, and H. Alloul, Pis'ma v ZhETF **99**, 542 (2014).
- ¹⁶ H. Alloul, I. R. Mukhamedshin, A. V. Dooglav, Y. V. Dmitriev, V. C. Ciomaga, L. Pinsard-Gaudart, and G. Collin, Phys. Rev. B **85**, 134433 (2012).
- ¹⁷ W. G. Clark, M. E. Hanson, F. Lefloch, and P. Segransan, Rev. Sci. Instrum. **66**, 2453 (1995).
- ¹⁸ A. P. Bussandri and M. J. Zuriaga, Journal of Magnetic Resonance **131**, 224 (1998).
- ¹⁹ A. Abragam, *The Principles of nuclear magnetism* (Oxford: Clarendon Press, London, 1961).
- ²⁰ C. P. Slichter, *Principles of Magnetic Resonance*, 3rd ed. (Springer-Verlag, Berlin, New York, 1990).
- ²¹ I. R. Mukhamedshin, H. Alloul, G. Collin, and N. Blanchard, Phys. Rev. Lett. **94**, 247602 (2005).
- ²² A. Abragam and F. Bleaney, *Electron Paramagnetic Resonance of Transition Ions* (Oxford: Clarendon Press, London, 1970).
- ²³ T. Kiyama and M. Itoh, Phys. Rev. Lett. **91**, 167202 (2003).
- ²⁴ G. Lang, J. Bobroff, H. Alloul, P. Mendels, N. Blanchard, and G. Collin, Phys. Rev. B **72**, 094404 (2005).
- ²⁵ C. de Vaulx, M.-H. Julien, C. Berthier, M. Horvatić, P. Bordet, V. Simonet, D. P. Chen, and C. T. Lin, Phys. Rev. Lett. **95**, 186405 (2005).
- ²⁶ In the point charge model calculations for the ^{59}Co quadrupole moment $Q=0.42$ and Sternheimer antishielding factor $\gamma = -7$ were used.
- ²⁷ J. W. Lynn, Q. Huang, C. M. Brown, V. L. Miller, M. L. Foo, R. E. Schaak, C. Y. Jones, E. A. Mackey, and R. J. Cava, Phys. Rev. B **68**, 214516 (2003).
- ²⁸ T. A. Platova, I. R. Mukhamedshin, H. Alloul, A. V. Dooglav, and G. Collin, Phys. Rev. B **80**, 224106 (2009).
- ²⁹ F.-T. Huang, M.-W. Chu, G. J. Shu, H. S. Sheu, C. H. Chen, L.-K. Liu, P. A. Lee, and F. C. Chou, Phys. Rev. B **79**, 014413 (2009).
- ³⁰ G. Khaliullin, Prog.Theor. Phys. Suppl. **160**, 155 (2005).
- ³¹ J. Chaloupka and G. Khaliullin, Prog.Theor. Phys. Suppl. **176**, 50 (2008).
- ³² S. Krivenko, Phys. Rev. B **85**, 064406 (2012).
- ³³ W. Koshibae and S. Maekawa, Phys. Rev. Lett. **91**, 257003 (2003).
- ³⁴ O. E. Peil, A. Georges, and F. Lechermann, Phys. Rev. Lett. **107**, 236404 (2011).
- ³⁵ T. A. Platova, I. R. Mukhamedshin, and A. V. Dooglav, in *Proceedings of XIV International Youth Scientific School "Actual Problems of Magnetic Resonance and its Application"*, Kazan, June 20-25, 2011, pp. 52–56.